The impact of concurrent variation of atmospheric meridional heat transport in western Baffen Bay and eastern Greenland on summer Arctic sea ice

Le Wang[1], Lujun Zhang[2*], Wenfa Yang[1]

[1] Hydrology Bureau, Yangtze River Water Resources Commission, Wuhan 430010, China

[2] School of Atmospheric Science, Nanjing University, Nanjing 210023, China

Abstract

Based on the climatological reanalysis data of the European Center for Medium-Range Weather Forecasts and the Arctic sea ice data of the National Snow and Ice Data Center, the relationship between the Arctic sea ice area (SIA) and the interannual variation of atmospheric meridional heat transport (AMHT) was analyzed. The results show that the atmospheric meridional heat transported by transient eddy (TAMHT) dominates the June AMHT in mid-high latitudes of the Northern Hemisphere, while the western Baffin Bay (B) and the eastern Greenland (G) are two gates for TAMHT entering the Arctic. TAMHT in the western Baffin Bay (B-TAMHT) and eastern Greenland (G-TAMHT) has a concurrent variation of reverse phase, which is closely related to the summer Arctic SIA. Possible mechanism is that the three Arctic atmospheric circulation patterns (AD, AO and NAO) in June can cause the concurrent variation of TAMHT in the B and G regions. This concurrent variation helps to maintain AD anomaly in summer through wave action and changes the polar air temperature, thus affecting the summer Arctic SIA. Calling the heat entering the Arctic as warm transport and the heat leaving Arctic as cold transport, then the results are classified into three situations based on B-TAMHT and G-TAMHT: warm B corresponding to cold G (WC), cold B corresponding to warm G (CW), cold B corresponding to cold G (CC), while warm B corresponding to warm G is virtually non-existent. During the WC situation, the SIA in the Pacific Arctic sediments and Kara Sea decreases; during the CW situation, the SIA in the Laptev Sea and Kara Sea decreases; during the CC situation, the SIA in the Kara Sea, Laptev Sea and southern Beaufort Sea increases.

Key words: Arctic, atmospheric meridional heat transport, transient eddy, sea ice, Arctic dipole

1 Introduction

The most visible change in the Arctic region in recent decades has been the rapid decline of the sea ice cover (Comiso et al., 2008; Comiso, 2012). As the most important cold source in the northern hemisphere, Arctic sea ice change has an important influence on the climate of the Arctic and even the Northern Hemisphere (Walsh, 2014; Overland et al., 2016; Liu et al., 2016), and the most important linkage between sea ice and climate is the atmospheric circulation (Deser and Teng, 2008; Zhang et al., 2008; Ogi and Wallace, 2007; Luo et al., 2016; Yao et al., 2017; He et al., 2018). Atmospheric circulation, the basic feature of the atmosphere, is formed by the unbalanced radiation energy absorbed by the earth's surface, which causes the atmospheric and oceanic heat fluxes flowing from the mid-low latitudes to the polar region. Many scholars have found that oceanic meridional energy transport plays an important role in the summer Arctic sea ice area (SIA) change (Polyakov et al., 2010; Woodgate et al., 2010), but there are relatively few studies on the atmospheric meridional heat transport (AMHT). In fact, in the Northern Hemisphere, the northward heat transported by the atmosphere and ocean is relatively close in low latitudes, but the main heat transport is from atmosphere in mid-high latitudes (Enderton and Marshall, 2009). That means AMHT is one of the important potential factors affecting Arctic sea ice.

According to the different transport forms, AMHT can be classified into three parts: mean meridional circulation transport, transient eddy transport and stationary eddy transport. In the mid-high latitudes of the northern hemisphere, the atmospheric meridional heat transported by transient eddy (TAMHT) dominates the poleward heat fluxes in summer (Oort, 1971), and it affects the Arctic climate through both thermodynamic and dynamic effects. For thermal effects, the summer Arctic atmospheric circulation pattern had a rapid change in recent decades, recognized as the Arctic Dipole (AD), which enhances water vapor and heat transport from mid-low latitudes to the Arctic (Wu et al., 2006; Overland et al., 2012). Moreover, the poleward atmospheric meridional energy transport in the northern hemisphere had an increasing trend in summer in the past 30 years, which heated up the Arctic troposphere atmosphere, thus contributing to the reduction of Arctic sea ice in summer (Kim and Choi, 2006; Graversen et al., 2008; Yoo et al., 2014; Yao et al., 2018; Zhang et al., 2012; Mewes and Jacobi, 2019); for dynamic effects, Arctic transi-

ent eddy mainly existed near major orography and blocking regions, primarily associated with the Pacific–North American (PNA) teleconnection and the Arctic Oscillation (AO) variability (Kwon and Joyce, 2013). It has a significant impact on polar atmospheric circulation, which will affect the Arctic sea ice (Hitchman et al., 1999; Luo, 2005; Kuroda, 2005; Lukovich and Barber, 2006; Simmonds and Keay, 2009; Shi and Bueh, 2011; Sung et al., 2016). Studies show that the blocking high anomaly over Greenland and Beaufort Sea in June is beneficial to export sea ice to the Atlantic Ocean (Overland and Wang, 2010), while the eddy activity of the lower atmosphere in late spring and early summer will also affect the summer Arctic SIA (Screen et al., 2011). The above studies show that AMHT has an important impact on the Arctic sea ice, and it is necessary to carry out further research on the relationship between them.

Currently, the research on the effect of AMHT on Arctic sea ice is mainly qualitative analysis, but there are relatively few studies have focused on the quantitative relationship, and the mechanism is not clear. This paper calculates the AMHT by using ECMWF reanalysis data, and links it to the Arctic sea ice. The purpose is to study the relationship between the AMHT and the summer Arctic sea ice, and analyze the underlying mechanism.

2 Data and methods

2.1 *Climate data*

The climate data used in this paper is the reanalysis data from European Center for Medium-Range Weather Forecasts (ECMWF) with a resolution of 1°×1°. This reanalysis data set is obtained by quality control and assimilation of observation data from various sources (ground, ship, radiosonde, wind balloon, aircraft, satellite, etc.) (Dee and Uppala, 2009). It is a comprehensive data set with many elements, wide range and long extension period. The elements include monthly mean sea-level pressure (MSLP), geopotential height, pressure, wind and air temperature, and the durations are 1979–2014.

Using three atmospheric circulation pattern to associate AMHT with Arctic sea ice, and they are the North Atlantic Oscillation (NAO), the Arctic Oscillation (AO) and the Arctic Dipole (AD). The AO and NAO indices are from NOAA/ National Weather Service-Climate Prediction Center (NOAA/NWS-CPC). The formal AD pattern has been defined as the second Empirical Orthogonal Function (EOF) of the MSLP anomaly north of 70°N, and its index is counted by ECMWF MSLP grid data.

2.2 *Sea ice data*

Satellite remote sensing technology plays an irreplaceable role in sea ice monitoring. The main method of global sea ice monitoring is to use microwave radiation brightness temperature data to retrieve the sea ice coverage, and then get the sea ice range and area (Comiso et al., 1997). Reliable sea-ice data were unavailable until 1979, when satellite observations began.

The sea ice concentration data used in this paper is provided by the National Snow and Ice Data Center (NSIDC, http://nsidc.org/data). It has been widely used in polar research and is one of the most recognized sea ice data in the world. NSIDC data is derived from scanning multichannel microwave radiometer (SMMR) mounted on Nimbus-7 and special sensor microwave/image (SSM/I) on the defense meteorological satellite program (DMSP) observations. The algorithms used are NASA team algorithm and bootstrap algorithm (Cavalieri et al., 1996; Comiso, 2000). We use monthly mean concentration data on a polar stereographic projection with a grid size of 25 km (the spatial grid is

304×448), and its duration is 1979–2014.

2.3 *Computation and decomposition of AMHT*

The atmospheric heat mainly includes sensible heat and latent heat. Sensible heat indicates the heat generated by the temperature change of the atmosphere, and latent heat indicates the heat generated by the phase change of water vapor in the atmosphere. The whole atmospheric meridional heat transport stream function can be defined in a general way as a function of pressure (Döös and Nilsson, 2011):

$$H(x,y,t) = \frac{1}{g} \int_{p_0}^{p_s} \left(c_p T(x,y,p,t) + Lq(x,y,p,t) \right) v(x,y,p,t) \mathrm{d}p, \quad (1)$$

where H is the whole atmospheric meridional heat transport at time t and location (x, y), x is the longitude, y is the latitude, t is the time, g is the gravitational constant, v is the meridional velocity, p_0 and p_s are pressures at the top and bottom of the atmosphere, T is the air temperature, and q is the specific humidity. $c_p T$ and Lq represent the sensible heat and latent heat in the atmosphere. Here, the temperature is measured in Kelvin and the constants used in the computations are the specific heat of dry air $c_p = 1\,004$ J/(kg · K) and the latent heat of evaporation $L = 2\,501$ J/g (taken as constant for simplicity).

According to the different transport forms, the meridional transport of atmosphere can be classified into three forms: mean meridional circulation transport, stationary eddy transport and transient eddy transport. The mean meridional circulation transport mainly represents the transport of the large-scale circulation field, and it can be counted with the mean value of variables for time and space; The stationary eddy transport can represent the transport of the trough and ridge, and the calculation method is the deviation of the time average of the variables from the zonal average; The transient eddy transport can represent the transport of the vortex in the atmosphere, and the calculation method is the deviation of the variables from the time average. The decomposition expressions are as follows (Oort, 1971):

$$\left[\overline{V\chi} \right] = \left[\bar{V} \right] \left[\bar{\chi} \right] + \left[\bar{V}^* \bar{\chi}^* \right] + \left[\overline{V'\chi'} \right], \quad (2)$$

$$\chi' = \chi - \bar{\chi}, \quad (3)$$

$$\chi^* = \chi - [\chi], \quad (4)$$

where the overbar represents time average and the [ ] represents the zonal average across all longitudes; the first term on the right side of Eq. (2) represents mean meridional circulation transport, the second term represents stationary eddy transport, and the third term represents transient eddy transport.

In order to analyze the relationship between the AMHT and the Arctic sea ice, the AMHT is classified into three parts. Combining Eq. (1) and Eq. (2) together, and the final decomposition formula of AMHT can be geted:

$$H_{\mathrm{mean}}(x,y,t) = \frac{1}{g} \int_{p_0}^{p_s} \left[\overline{v(x,y,p,t)} \right] \left[\overline{\chi(x,y,p,t)} \right] \mathrm{d}p, \quad (5)$$

$$H_{\text{seddy}}(x, y, t) = \frac{1}{g} \int_{p_0}^{p_s} \left[\overline{v(x, y, p, t)^*} \; \overline{\chi(x, y, p, t)^*} \right] \mathrm{d}p, \quad (6)$$

$$H_{\text{teddy}}(x, y, t) = \frac{1}{g} \int_{p_0}^{p_s} \left[\overline{v(x, y, p, t)' \chi(x, y, p, t)'} \right] \mathrm{d}p, \quad (7)$$

$$\chi(x, y, p, t) = c_p T(x, y, p, t) + Lq(x, y, p, t), \quad (8)$$

where H_{mean} represents atmospheric meridional heat transported by mean meridional circulation, H_{seddy} represents heat transported by stationary eddy, and H_{teddy} represents heat transported by transient eddy.

Graversen et al. (2008) found that the AMHT across 60°N latitude could effectively represent the heat fluxes from mid-low latitudes to the polar region. Therefore, we chose AMHT of 60°N to represent the poleward heat transport. In this paper, AMHT and TAMHT refer to the whole atmospheric heat at 60°N unless otherwise specified. The Arctic summer is defined as June to September because the Arctic SIA is minimum in September.

3 Results and discussion

### 3.1 *Relationship between AMHT and Arctic sea ice*

Calculating three different types of AMHT (Table 1) in the summer half year (May-October) of 1979–2014. It was found that in the past 36 years, the TAMHT dominated the atmospheric poleward heat transport in mid-high latitudes in summer half year (accounting for 64%), which was consistent with the research of Oort (1971). Therefore, the relationship between TAMHT and summer (June to September) Arctic sea ice was mainly analyzed. Through analysis of the correlation coefficients between leading TAMHT and summer Arctic SIA (Fig. 1), it is found that the June TAMHT was significantly related to the summer SIA of the Beaufort Sea, while the TAMHT in May and July had a poor correlation (The correlation in January–April and Au-

gust–September is also poor). For the convenience of analysis, the significant correlation area between June TAMHT and summer SIA was taken as a key region (72°–85°N, 180°–120°W, shown in the red box of Fig. 1). The correlation coefficient between June TAMHT and summer SIA in key region (KSIA) was found to be as high as –0.54 (after detrend is –0.47) and passed 99% confidence level. That indicates the TAMHT in June is closely related to the KSIA in summer.

The correlation coefficients between TAMHT in June and summer SIA by each month were also calculated. The summer SIA was divided into June SIA, July SIA, August SIA and September SIA (Fig. 2). It could be seen that from June to September, there was a large-scale significant negative correlation area on the side of the Arctic Pacific sector. In June and July, the significant negative correlation area was located in the Beaufort Sea; in August, it was located in the north seas of Beaufort Sea and Canadian islands; and in September, the area was reduced, mainly located in the northern part of the Beaufort Sea and Chukchi Sea. Generally speaking, from June to September, the area of significant negative correlation between SIA and June TAMHT showed a trend of increasing first and then decreasing, and the largest area appeared in August.

Affected by external forcing and atmospheric instability, the distribution of TAMHT is not uniform in the zonal and vertical directions. So it is necessary to analyze the relationship between TAMHT and summer KSIA from different directions. The correlation coefficients between the summer KSIA and the zonal TAMHT in June are shown in Fig. 3a. There was one significant positive correlation region in 35°–50°W and one negative correlation region in 60°–90°W, respectively, while the correlation in other longitudes was poor. TAMHT in the two regions, which corresponding to the eastern Greenland and the western Baffin Bay, are called as G-TAMHT and B-TAMHT. Figure 3b is the correlation in the vertical direction between the TAMHT and the KSIA. The B-TAMHT at 1 000–300 hPa was negatively correlated with summer KSIA, while G-TAMHT at 800–300 hPa and above 100 hPa was positively correlated with summer KSIA. That is consistent with the conclusion of Fig. 3a. In order to study the reasons for

Table 1. Three different types of AMHT and their proportions in the summer half year of 1979–2014

|	Transient eddy	Stationary eddy	Mean meridional circulation
Heat value/J	3.164×10^5	7.70×10^4	9.75×10^4
Percentage/%	64	16	20
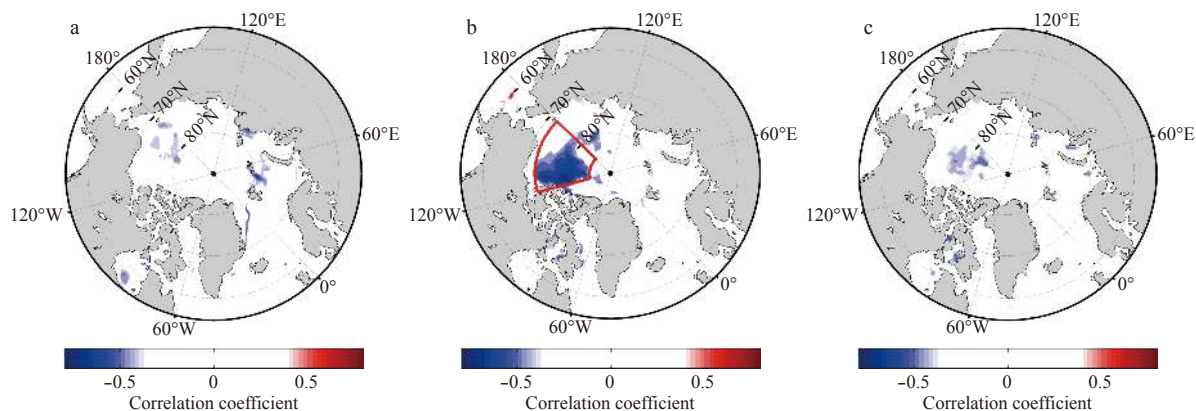
Fig. 1. The spatial distribution of correlation coefficients between zonal mean TAMHT of 60°N latitude and summer (June to September) Arctic SIA from 1979 to 2014. a. May, b. June and c. July. The confidence level of shade is above 0.05.
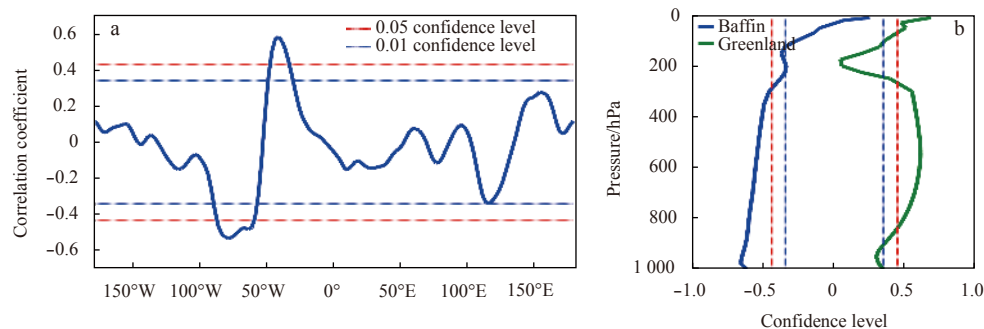
this inverse correlation, the time series of B-TAMHT and G-TAM-HT in June in recent 36 years are given in Fig. 4a. It can be seen that the B-TAMHT in June had a decreasing trend before 1990 and an obvious increasing trend after 1995, while the G-TAMHT had an increasing trend before 1990 and an obvious decreasing trend after 1995. The correlation coefficient of the two is as high

as –0.78, meaning a good correspondence between peak and valley. This shows that in the past 36 years, when the heat entering the polar region from the B region increased, the heat leaving the polar region from the G region usually increased, and vice versa.

Since the June B-TAMHT and G-TAMHT had a reverse phase change, how was AMHT transported in the polar region? The
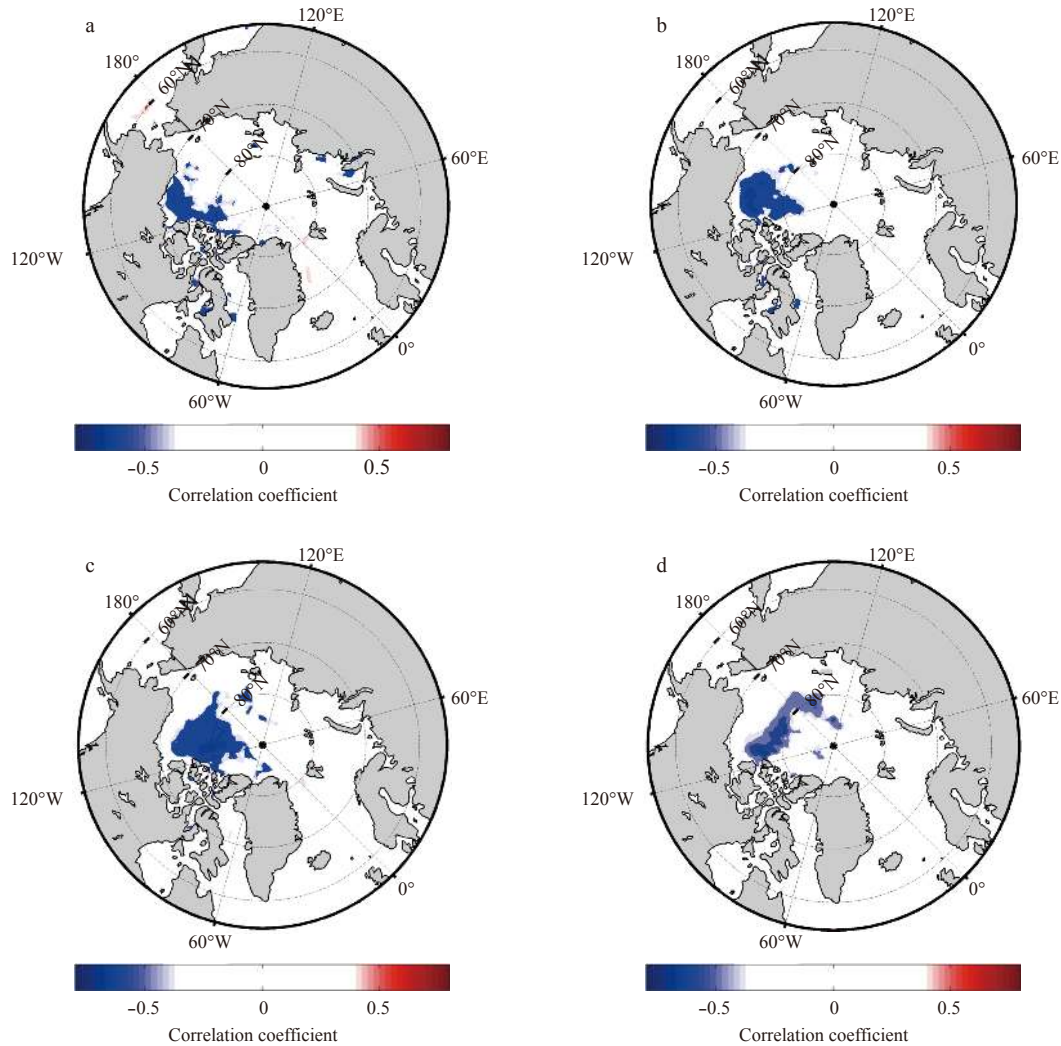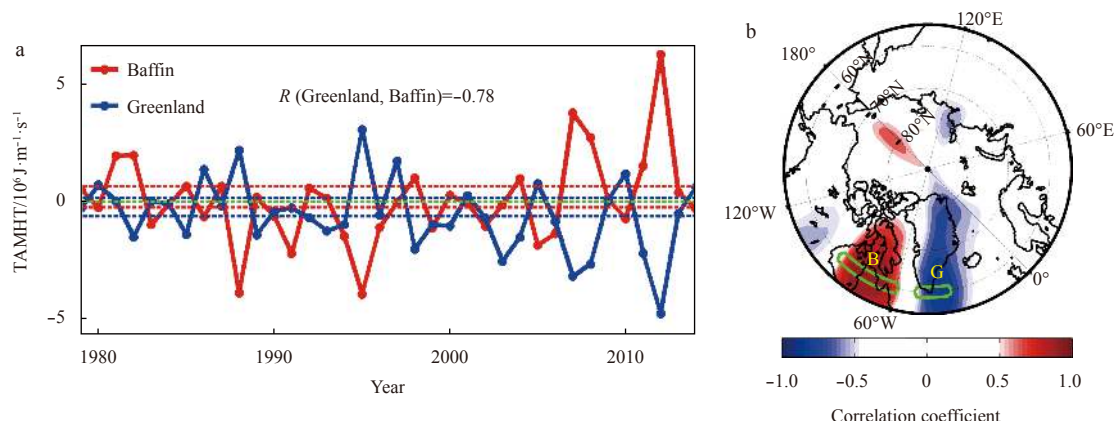

Fig. 2. The spatial distribution of correlation coefficients between zonal-mean TAMHT of 60°N latitude and summer Arctic SIA by each month from 1979 to 2014. a. June, b. July, c. August, and d. September. The confidence level of shade is above 0.05.

Fig. 3. The correlation between KSIA in summer and TAMHT at 60°N (a) and B-TAMHT and G-TAMHT in vertical direction (b) in June.

Fig. 4. Time series of B-TAMHT and G-TAMHT in June (a) (dashed red and blue lines indicate the 30% percentile and 70% percentile of B-TAMHT and G-TAMHT, respectively) and spatial distribution of correlation coefficient between B-TAMHT and Arctic TAMHT on grid in June (b) (the shade is the correlation cofficient whose confidence level is above 0.05 and the green box is the extent of the B area and G area).

spatial distribution of correlation coefficients between June B-TAMHT and June Arctic TAMHT on the grid is shown in Fig. 4b. Positive values appeared over the Baffin Bay and 180° meridian in polar region, and negative values appeared over the Greenland. This indicates that the TAMHT enters the polar region from the Baffin Bay and leaves the Arctic along the northern North American–the Beaufort Sea–the center of the polar–the eastern Greenland, while the TAMHT enters the polar region from the eastern Greenland and leaves the Arctic along the opposite route. We found there was no significant correlation coefficient over the northern North American in Fig. 4b, because the heat in that area mainly moved along the latitudinal direction.

3.2 *Circulation background of TAMHT affecting Arctic sea ice*

Correlation analysis shows that the concurrent variation of G-TAMHT and B-TAMHT in June corresponds well with the inter-annual changes of the KSIA in summer, so it is necessary to analyze the circulation background based on the TAMHT anomalous years. Through dividing TAMHT into warm and cold transport, where warm means transporting heat to Arctic and cold means exporting heat from the Arctic, the TAMHT anomaly could be divided into warm and cold anomaly, and the anomalous years could be selected. We calculated the 30% percentile and 70% percentile of B-TAMHT and G-TAMHT, respectively, and took them as the thresholds of warm and cold anomalous

years (red and blue dashed lines in Fig. 4a). When B-TAMHT was greater than its 70% percentile (6.03×10^5 J/(m·s)), it was a warm B-TAMHT anomalous year. And when it was less than its 30% percentile (-1.12×10^5 J/(m·s)), it was a cold B-TAMHT anomalous year. And G-TAMHT anomalous years were selected with the same way (70% quantile is 4.87×10^4 J/(m·s) and 30% quantile is -5.88×10^5 J/(m·s)). The results are classified into four situations based on TAMHT anomaly years in the two regions (Table 2): warm B corresponding to cold G (WC), cold B corresponding to warm G (CW), cold B corresponding to cold G (CC), and warm B corresponding to warm G (WW). It is noteworthy that there was no year in which B-TAMHT and G-TAMHT were both warm in the past 36 years (Table 2). And that indicates, in the past 36 years, there was no case that the western Baffin Bay and the eastern Greenland simultaneously transported large amounts of transient heat to the polar region in June.

The spatial distribution of June TAMHT in the three scenarios was shown in Fig. 5. In the WC and CW scenarios, heat ex-

Table 2. The anomalous years of TAMHT in June

	Anomalous years
B-TAMHT+G-TAMHT−(WC)	1982, 1998, 2004, 2007, 2008, 2011, 2012
B-TAMHT−G-TAMHT+(CW)	1986, 1988, 1995, 2005, 2010
B-TAMHT+G-TAMHT+(OO)	–
B-TAMHT−G-TAMHT−(CC)	1994, 1999, 2002, 2003, 2006
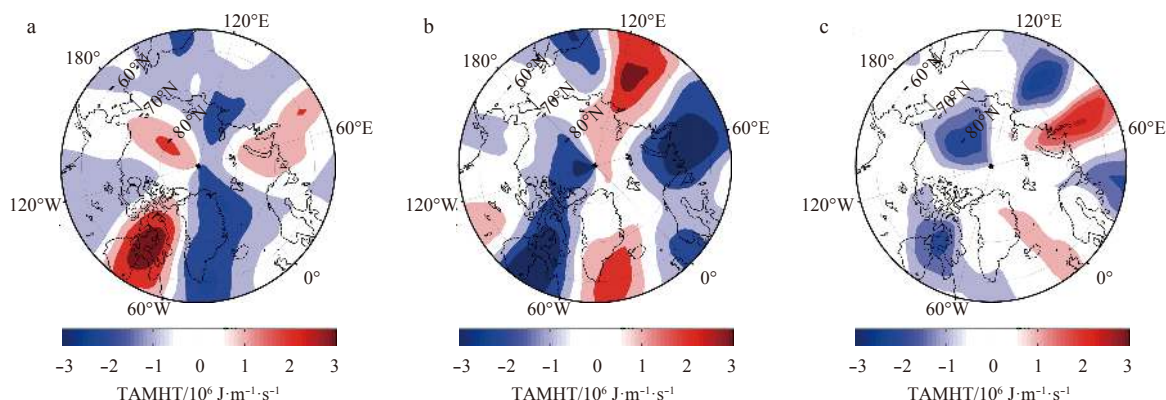
Fig. 5. Composite of TAMHT in June in the three scenarios. a. WC, b. CW and c. CC.

change between the Arctic and mid-latitudes was very strong. In the case of WC, the B and G regions were the most important channels for the transient heat transport to the polar region. In the CW case, the B and G regions were the main channels on the Atlantic side for TAMHT, and in addition, there were two main channels on the Eurasian continent. In the case of CC, the B-TAMHT extended to G region as a ring shape, while the G-TAM-HT weakened and moved eastward, so both the B and G regions lost heat at 60°N. At this time, the heat exchange between the Arctic and middle latitudes significantly weakens, and the entire polar region has a relatively closed state. This is conducive to the accumulation of cold air in the polar region, which contributes to

the increase of SIA.

Figure 6 shows the results of the composite analysis based on the three situations. During the WC situation, heat entered the Arctic from the western Baffin Bay and left the Arctic from the eastern Greenland. It was found that there was warm air over the Pacific Arctic sediments and Kara Sea (Fig. 6g), and high pressure anomaly over the Arctic Ocean and Greenland, and low pressure anomaly over the continents and oceans beyond the Arctic Ocean in summer (Figs 6a, d). This is conductive to the formation of floating ice by melting sea ice in the Pacific Arctic sediments and Kara Sea, and the floating ice is exported to the Atlantic Ocean through anticyclone circulation in the polar re-
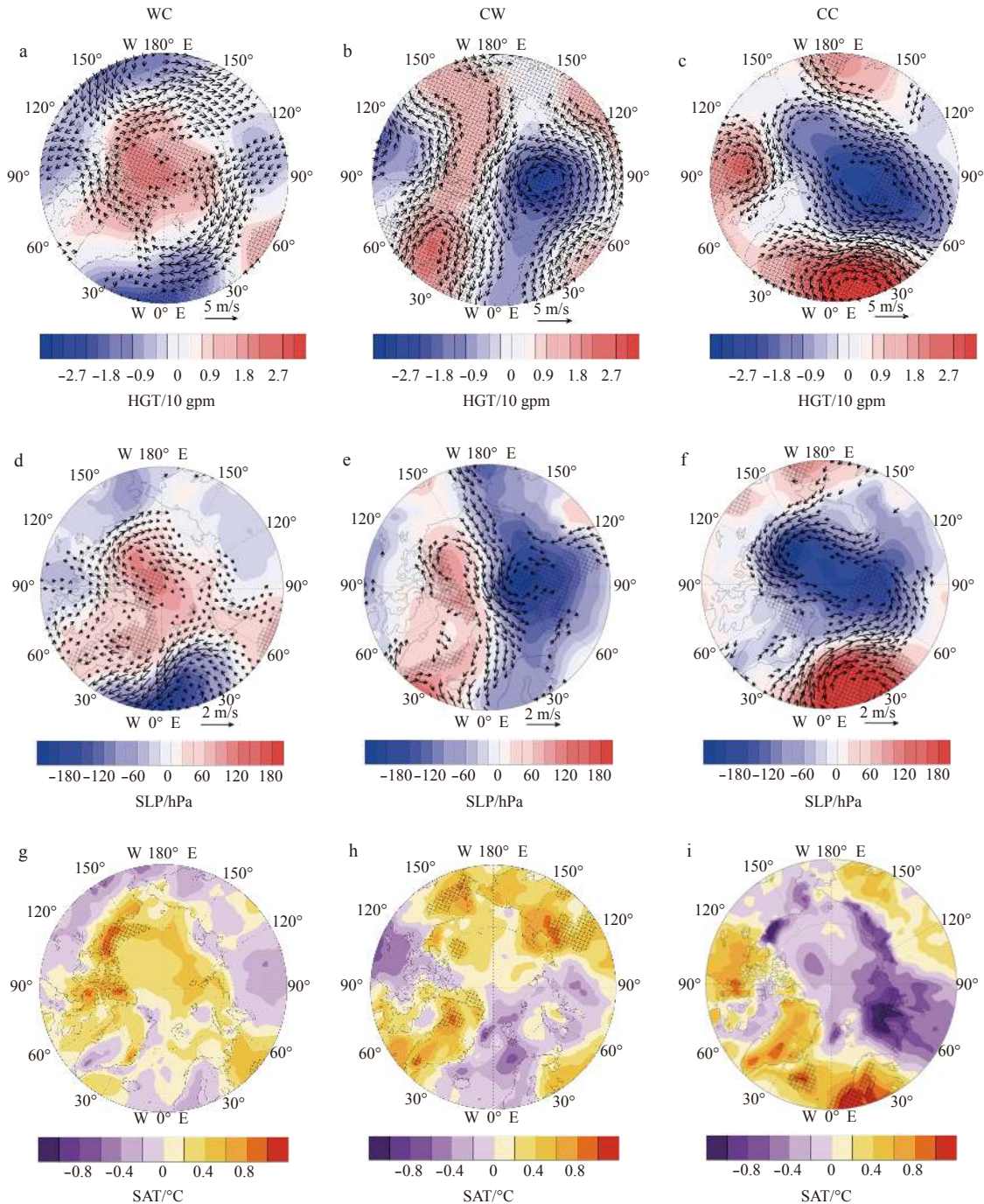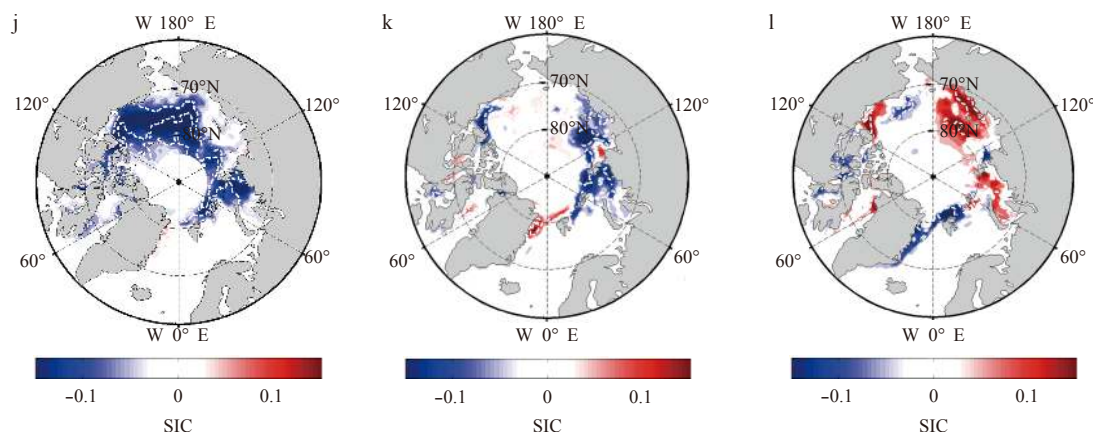

Fig. 6.

Fig. 6. Composite 500 hPa geopotential height (HGT) and horizontal wind (a–c), sea level pressure (SLP) and 10 m wind (d–f), surface air temperature (SAT) (g–i), and sea ice concentration (SIC) (j–l) in summer. The confidence level of squares, arrows and white dotted line is above 0.1.

gion. Finally, sea ice in the Pacific Arctic sediments and the Kara Sea is reduced (Fig. 6l). During the CW situation, heat entered the Arctic from the eastern Greenland and left the Arctic from the western Baffin Bay. We found relatively warm air over the Pacific Arctic sediments, especially over the Laptev Sea (Fig. 5h), and low pressure anomaly over the Siberia, high pressure anomaly over the Beaufort Sea and Greenland, and strong transpolar drift over the central Arctic Ocean in summer (Figs 6b, e). The cyclonic circulation in northern Siberia transports the sea ice from the Kara Sea to the Laptev Sea, which helps to melt sea ice in the Laptev Sea. And the strong transpolar drift enhances the output of Arctic sea ice to the Atlantic Ocean. As a result, sea ice in the Laptev Sea and Kara Sea is reduced (Fig. 6k). During the CC situation, heat left the Arctic from both the western Baffin Bay and the eastern Greenland. It was found that there was cold air over the Kara Sea (Fig. 6i), Laptev Sea and southern Beaufort Sea and low pressure anomaly over the center part of the polar region and Greenland. The cold air makes sea ice growth and the low pressure lock sea ice in the Arctic Ocean (Figs 6c, f), which resulting in more sea ice in the Kara Sea, Laptev Sea and southern Beaufort Sea (Fig. 6l).

Generally speaking, when the B-TAMHT and G-TAMHT are in reverse phase in June, the temperature in the polar region increases abnormally, and the atmospheric circulation pattern is similar to negative AD phase, which contributes to the reduction of sea ice. When both B-TAMHT and G-TAMHT are cold in June, the corresponding circulation situation is contrary to the above situation, resulting in the increase of sea ice.

3.3 *Concurrent variation index and possible mechanism*

The composite analysis shows that the effects of B-TAMHT and G-TAMHT on Arctic sea ice in June are complex. The single B-TAMHT or G-TAMHT cannot fully indicate the combined effects of them. So we define an index reflecting the concurrent variation of them, and quantitatively study the relationship between the concurrent variation of TAMHT and Arctic sea ice. The index is calculated as follows:

$$H = \frac{-b \times g\,(|g| + |b|)}{|b \times g|},\tag{9}$$

where b is the B-TAMHT and g is the G-TAMHT, $(|g| + |b|)$ is the

size term, and $\dfrac{-b \times g}{|b \times g|}$ is the symbol term. When B-TAMHT and G-TAMHT are reverse, the corresponding circulation is beneficial to the reduction of sea ice, and the definition index is positive. When both of them are cold, the corresponding circulation is contrary to the former, and the definition index is negative. Since the situation of both being warm is basically absent, this situation is not considered in the formula. It is noteworthy that the H index is standardized in the following paper.

To verify the relationship between H index and summer Arctic sea ice, a linear regression analysis of summer Arctic SIA field on standardized H index was conducted (Fig. 7). The results show that when the H index increased, the sea ice in the Pacific Arctic sediments and Kara Sea decreased significantly. The correlation coefficient between the H and the KSIA (Fig. 1b) is –0.63, significantly higher than it in Fig. 1b (–0.54), and the range of negative correlation is much larger. That indicates the defined H
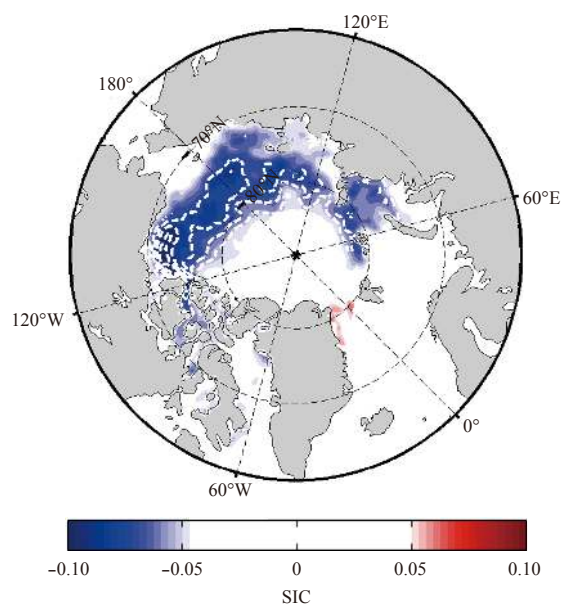
Fig. 7. Summer Arctic sea ice concentration (SIC) regressed linearly on the H index for the period of 1979–2014. The confidence level of contours is 0.05.

index can better reflect the relationship between the June TAM-HT concurrent variation and the summer Arctic sea ice.

Then, what is the physical mechanism of this phenomenon? TAMHT in the polar region is mainly distributed near the large terrain and high pressure (Kwon and Joyce, 2013), and it is closely related to atmospheric circulation patterns (Sung et al., 2016; Serreze and Barrett, 2008; Simmonds et al., 2008). In recent years, the Arctic pressure field and wind field had changed continuously in June. The Siberian pressure was abnormally low compared with climatology, and the pressure in the Beaufort Sea, North America and Greenland was abnormally high compared with climatology. This atmospheric circulation type is called AD negative phase, which is conducive to enhance the meridional circulation (Overland et al., 2012). Since B-TAMHT and G-TAMHT are located on the east and west sides of Greenland in June, corresponding to the high pressure in the negative phase of AD, it can be speculated that the concurrent variation of B-TAMHT and G-TAMHT may be related to the AD circulation pattern.

To verify this conjecture, the AD, AO and NAO index were used to correlate with standardized *H* index during 1979–2014 (Table 3). In May, the correlation between the three indices and *H* were all poor. In June, the AD index had the highest correlation with *H* (the correlation coefficient is –0.51), and the correlation of AO and NAO were also high (the correlation coefficient is –0.43 and 0.46, respectively). It meant that negative phase of the three atmospheric usually corresponded to the inverse phase of B-TAMHT and G-TAMHT, while the positive phase usually corresponded to the cold B-TAMHT and G-TAMHT. And among them, the AD pattern had the greatest impact, followed by NAO and AO, respectively. In July and August, only AD index was significantly negatively correlated with *H*. In September, the correlation was all poor, that meant the sea ice in September was mainly influenced by the early atmospheric circulation pattern. The summer average results showed that the AD index had the highest negative correlation with *H* (–0.47, passing the 99% confidence level), followed by NAO (–0.38, passing the 95% confidence level), and finally AO (–0.19, correlation is not significant). The above analysis proves that the three atmospheric circulation patterns in June can affect the occurrence of concurrent variation of TAMHT, and then the TAMHT is conducive to the maintenance of the AD pattern during June to August.

Figure 8 shows the difference of positive and negative AO, NAO and AD related to the TAMHT in June. It is found that the

Table 3. The correlation coefficients between *H* index and three atmospheric circulation pattern index

	May	Jun.	Jul.	Aug.	Sep.	JJAS
AD	0.01	**–0.51***	**–0.4**	**–0.32**	–0.13	**–0.47***
AO	–0.28	**–0.43***	–0.2	0.02	0.25	–0.19
NAO	–0.14	**–0.46***	–0.29	–0.27	0.14	**–0.38**

Note: Bold represents passing the 95% confidence level and asterisk (*) represents passing the 99% confidence level.

distributions of TAMHT of the three circulation patterns are similar. In the positive mode, the B region shows an obvious cold transport, while the G region shows a weaker cold transport, which corresponding a negative *H* index. In the negative mode, a strong warm transport appears on the B region, while a strong cold transport appears on the G region, and this reverse heat distribution corresponds to a positive *H* index. It is consistent with the conclusion in Table 3, which further proves that the negative anomalies of three Arctic atmospheric circulation patterns in June are beneficial to the antiphase concurrent variation of TAMHT in western Baffin Bay and eastern Greenland.

Many scholars pointed out that the transient eddies could cause anomalous change of the polar vortex and the sea level pressure in the polar region through wave action, which obviously affected the Arctic atmospheric circulation pattern (Hitchman et al., 1999; Simmonds et al., 2008; Lukovich and Barber, 2006; Shi and Bueh, 2011). Therefore, the regression analysis of summer air pressure and temperature field on standardized *H* index was shown in Fig. 9. When the *H* index increased, high pressure anomalies appeared over the Beaufort Sea, polar center and Greenland, and low pressure anomalies appeared over the North America and Eurasia (Figs 9a and b). This likes a typical negative phase of AD, helping to transport Arctic sea ice to the Atlantic (Wu et al., 2006; Wang et al., 2009; Overland et al., 2012), which indicates that the concurrent variation of TAMHT in June is conducive to the maintenance of the AD pattern in summer. The regression analysis of temperature (Fig. 9c) showed that when the *H* index increased, the temperature along the northern coast of North America and Eurasia increased, resulting in the reduction of SIA.

The above results prove that the three atmospheric circulation patterns in June can cause the concurrent variation of B-TAMHT and G-TAMHT, and the concurrent variation is beneficial to the maintenance of typical AD pattern from June to Au-
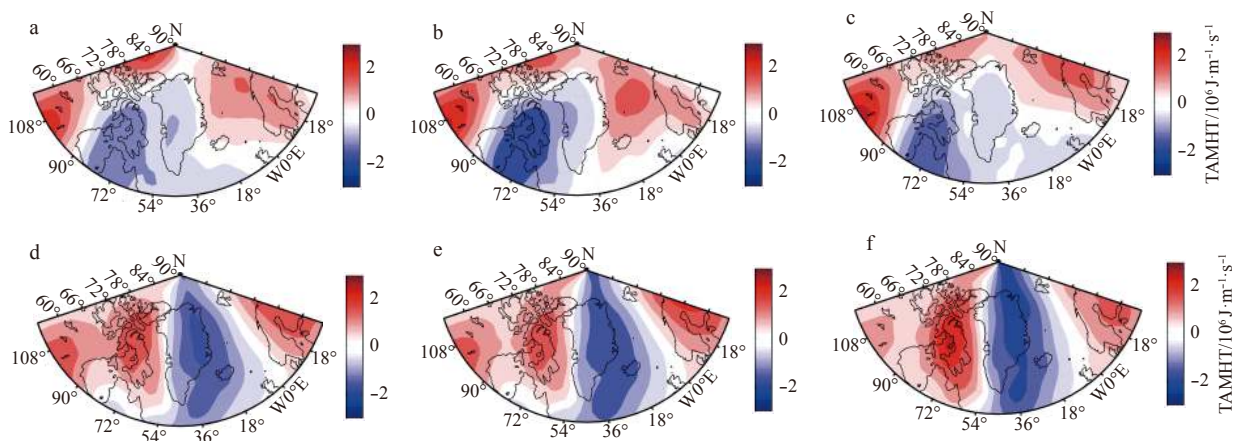
Fig. 8. Composite TAMHT under three kinds of Arctic atmospheric circulation anomaly in June. a. Positive AO, b. positive NAO, c. positive AD, d. negative AO, e. negative NAO, and f. negative AD.
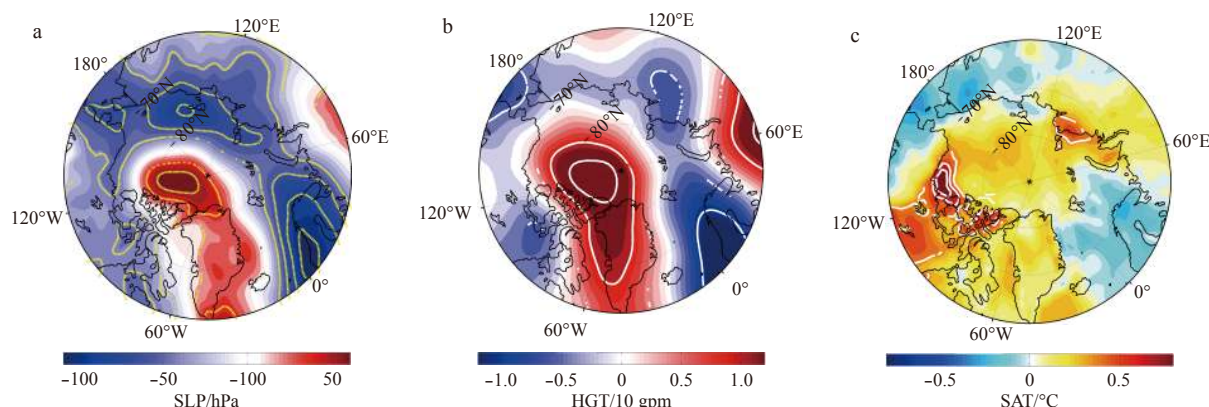
Fig. 9. Summer Arctic climatic factors regressed linearly on the standardized *H* index for the period of 1979–2014. a. Sea level pressure, b. 500 hPa geopotential height and c. surface air temperature. The confidence level of contours is 0.05.

gust, finally resulting in the variation of summer Arctic SIA.

4 Conclusions

In this paper, the impact of AMHT on summer Arctic sea ice during the period of 1979-2014 is studied. The results show that the TAMHT concurrent variation in the Greenland and Baffin Bay in June is closely related to summer Arctic sea ice. We defined the concurrent variation index *H*, and found it could better reflect the negative correlation with summer Arctic SIA. The possible mechanism is that the three typical Arctic atmospheric circulation patterns (AD, AO, NAO) in June can lead to a concurrent variation of TAMHT in the western Baffin Bay and the eastern Greenland (Impact of AD is the most important), and then this concurrent variation causes the maintenance of AD pattern from June to August. The negative patterns of AD/NAO/AO in June usually cause the reverse change of B-TAMHT and G-TAMHT, which are divided into two situations: (1) When transient heat enters the Arctic from the western Baffin Bay and leaves the Arctic from the eastern Greenland, the air over the Pacific Arctic sediments and the Kara Sea will be heated. The transient eddies weaken the polar vortices and enhance the sea level pressure in the polar region through wave action, making the polar region maintain a circulation pattern similar to the negative AD from June to August. Under this pattern, sea ice in the Pacific Arctic sediments and Kara Sea will melt and form floating ice, and the sea ice will be exported to the Atlantic through the anticyclone circulation in the center part of polar region. (2) When the transient heat enters the Arctic from the eastern Greenland and leaves the Arctic from the western Baffin Bay, the thermal effect of TAMHT is weak, mainly heating the atmosphere of Laptev Sea. The transient eddies increase the pressure in the western polar region and weaken the pressure in the eastern polar region through wave action, which make the polar region maintain an obvious negative AD phase from June to August. Under this circulation pattern, strong transpolar drift appears in the central part of the Arctic Ocean, and the cyclonic gyre in northern Siberia transports sea ice of the Kara Sea to the Laptev Sea. This is conductive to melt ice in the Laptev Sea, and the sea ice is exported to the Atlantic Ocean through transpolar drift, finally resulting in the reduction of sea ice in the Laptev Sea and Kara Sea; When the positive patterns of AD/NAO/AO appears in June, it usually causes both B-TAMHT and G-TAMHT exporting heat from Arctic. The physical mechanism of this situation is contrary to the above situation. The concurrent variation of B-TAMHT and G-TAMHT

in June helps to maintain the positive AD in summer, which leads to more sea ice in the southern Beaufort Sea, Kara Sea and Laptev Sea.

Many scholars have studied the impacts of atmospheric circulation on summer Arctic sea ice variation on different time scales (Deser and Teng, 2008; Zhang et al., 2003; Ogi and Wallace, 2007; Rigor et al., 2002; Zhang et al., 2008). However, there are few studies on the effects of AMHT on the Arctic sea ice. In fact, in recent years, with the change of atmospheric circulation patterns, the exchange of material and energy between polar regions and mid-low latitudes has become more frequent (Zhang et al., 2012; Overland and Wang, 2010). The local thermodynamic processes in polar region are not enough to explain the causes of the rapid changes of Arctic sea ice in summer, which requires us to focus more on the telecorrelation between mid-low latitudes and Arctic sea ice. AMHT is one of the most important linkages between mid-low latitudes and polar region. In this paper, we find that the concurrent variation of TAMHT in June affects summer Arctic sea ice by affecting summer atmospheric circulation. This conclusion supplements the knowledge of ice-air interaction, but the relationship between TAMHT and Arctic sea ice is verified only by statistical methods, while the dynamic mechanism of TAMHT affecting atmospheric circulation is not clearly explained. These problems need to be further studied in future work.

References

Cavalieri D, Parkinson C, Gloersen P, et al. 1996. Sea ice concentrations from Nimbus-7 SMMR and DMSP SSM/I-SSMIS passive microwave data. Boulder, Colorado, USA: NASA DAAC at the National Snow and Ice Data Center

Comiso J C. 2000. Bootstrap sea ice concentrations from Nimbus-7 SMMR and DMSP SSM/I-SSMIS, Version 2. Boulder, Colorado, USA: NASA National Snow and Ice Data Center Distributed Active Archive Center

Comiso J C. 2012. Large decadal decline of the Arctic multiyear ice cover. Journal of Climate, 25(4): 1176–1193, doi: 10.1175/JCLI-D-11-00113.1

Comiso J C, Cavalieri D J, Parkinson C L, et al. 1997. Passive microwave algorithms for sea ice concentration: a comparison of two techniques. Remote Sensing of Environment, 60(3): 357–384, doi: 10.1016/S0034-4257(96)00220-9

Comiso J C, Parkinson C L, Gersten R, et al. 2008. Accelerated decline in the arctic sea ice cover. Geophysical Research Letters, 35(1): L01703

Dee D P, Uppala S. 2009. Variational bias correction of satellite radiance data in the ERA-Interim reanalysis. Quarterly Journal of the Royal Meteorological Society, 135(644): 1830–1841, doi:

10.1002/qj.493

Deser C, Teng Haiyan. 2008. Evolution of Arctic sea ice concentration trends and the role of atmospheric circulation forcing, 1979–2007. Geophysical Research Letters, 35(2): L02504

Döös K, Nilsson J. 2011. Analysis of the meridional energy transport by Atmospheric overturning circulations. Journal of the Atmospheric Sciences, 68(8): 1806–1820, doi: 10.1175/2010JAS3493.1

Enderton D, Marshall J. 2009. Explorations of Atmosphere-Ocean-Ice climates on an aquaplanet and their meridional energy transports. Journal of the Atmospheric Sciences, 66(6): 1593–1611, doi: 10.1175/2008JAS2680.1

Graversen R G, Mauritsen T, Tjernström M, et al. 2008. Vertical structure of recent Arctic warming. Nature, 451(7174): 53–56, doi: 10.1038/nature06502

He Shengping, Knudsen E M, Thompson D W J, et al. 2018. Evidence for predictive skill of high-latitude climate due to midsummer sea ice extent anomalies. Geophysical Research Letters, 45(17): 9114–9122, doi: 10.1029/2018GL078281

Hitchman M H, Buker M L, Tripoli G J. 1999. Influence of synoptic waves on column ozone during Arctic summer 1997. Journal of Geophysical Research: Atmospheres, 104(D21): 26547–26564, doi: 10.1029/1999JD900471

Kim D, Choi W. 2006. Decadal and year-to-year variations of the Arctic lower-stratospheric temperature for the month of March and their relationship with eddy heat flux. International Journal of Climatology, 26(8): 1125–1132, doi: 10.1002/joc.1312

Kuroda Y. 2005. On the influence of the meridional circulation and surface pressure change on the Arctic Oscillation. Journal of Geophysical Research: Atmospheres, 110(D21): D21107, doi: 10.1029/2004JD005743

Kwon Y O, Joyce T M. 2013. Northern hemisphere winter atmospheric transient eddy heat fluxes and the Gulf Stream and Kuroshio-Oyashio extension variability. Journal of Climate, 26(24): 9839–9859, doi: 10.1175/JCLI-D-12-00647.1

Liu Na, Lin Lina, Wang Yingjie, et al. 2016. Arctic autumn sea ice decline and Asian winter temperature anomaly. Acta Oceanologica Sinica, 35(7): 36–41, doi: 10.1007/s13131-016-0911-0

Lukovich J V, Barber D G. 2006. Atmospheric controls on sea ice motion in the southern Beaufort Sea. Journal of Geophysical Research: Atmospheres, 111(D18): D18103, doi: 10.1029/2005JD006408

Luo Dehai. 2005. A barotropic envelope Rossby Soliton model for block-eddy interaction: Part I. Effect of topography. Journal of the Atmospheric Sciences, 62(1): 5–21, doi: 10.1175/1186.1

Luo Dehai, Xiao Yiqing, Yao Yao, et al. 2016. Impact of Ural Blocking on winter warm Arctic-cold Eurasian anomalies: Part I. Blocking-induced amplification. Journal of Climate, 29(11): 3925–3947, doi: 10.1175/JCLI-D-15-0611.1

Mewes D, Jacobi C. 2019. Heat transport pathways into the Arctic and their connections to surface air temperatures. Atmospheric Chemistry and Physics, 19(6): 3927–3937, doi: 10.5194/acp-19-3927-2019

Ogi M, Wallace J M. 2007. Summer minimum Arctic sea ice extent and the associated summer atmospheric circulation. Geophysical Research Letters, 34(12): L12705, doi: 10.1029/2007GL029897

Oort A H. 1971. The Observed annual cycle in the meridional transport of atmospheric energy. Journal of the Atmospheric Sciences, 28(3): 325–339, doi: 10.1175/1520-0469(1971)028<0325:TOACIT>2.0.CO;2

Overland J E, Dethloff K, Francis J A, et al. 2016. Nonlinear response of mid-latitude weather to the changing Arctic. Nature Climate Change, 6(11): 992–999, doi: 10.1038/nclimate3121

Overland J E, Francis J A, Hanna E, et al. 2012. The recent shift in early summer Arctic atmospheric circulation. Geophysical Research Letters, 39(19): L19804

Overland J E, Wang Muyin. 2010. Large-scale atmospheric circulation changes are associated with the recent loss of Arctic sea ice. Tellus A, 62(1): 1–9, doi: 10.1111/j.1600-0870.2009.00421.x

Polyakov I V, Timokhov L A, Alexeev V A, et al. 2010. Arctic Ocean warming contributes to reduced polar ice cap. Journal of Physical Oceanography, 40(12): 2743–2756, doi: 10.1175/2010JPO4339.1

Rigor I G, Wallace J M, Colony R L. 2002. Response of sea ice to the Arctic Oscillation. Journal of Climate, 15(18): 2648–2663, doi: 10.1175/1520-0442(2002)015<2648:ROSITT>2.0.CO;2

Screen J A, Simmonds I, Keay K. 2011. Dramatic interannual changes of perennial arctic sea ice linked to abnormal summer storm activity. Journal of Geophysical Research: Atmospheres, 116(D15): D15105, doi: 10.1029/2011JD015847

Serreze M C, Barrett A P. 2008. The summer cyclone maximum over the central Arctic Ocean. Journal of Climate, 21(5): 1048–1065, doi: 10.1175/2007JCLI1810.1

Shi Ning, Bueh C. 2011. Two types of Arctic oscillation and their associated dynamic features. Atmospheric and Oceanic Science Letters, 4(5): 287–292, doi: 10.1080/16742834.2011.11446944

Simmonds I, Burke C, Keay K. 2008. Arctic climate change as manifest in cyclone behavior. Journal of Climate, 21(22): 5777–5796, doi: 10.1175/2008JCLI2366.1

Simmonds I, Keay K. 2009. Extraordinary September Arctic sea ice reductions and their relationships with storm behavior over 1979–2008. Geophysical Research Letters, 36(19): L19715, doi: 10.1029/2009GL039810

Sung M K, Kim B M, Baek E H, et al. 2016. Arctic-North Pacific coupled impacts on the late autumn cold in North America. Environmental Research Letters, 11(8): 084016, doi: 10.1088/1748-9326/11/8/084016

Walsh J E. 2014. Intensified warming of the Arctic: Causes and impacts on middle latitudes. Global and Planetary Change, 117: 52–63, doi: 10.1016/j.gloplacha.2014.03.003

Wang Jia, Zhang Jinlun, Watanabe E, et al. 2009. Is the Dipole Anomaly a major driver to record lows in Arctic summer sea ice extent?. Geophysical Research Letters, 36(5): L05706

Woodgate R A, Weingartner T, Lindsay R. 2010. The 2007 Bering Strait oceanic heat flux and anomalous Arctic sea-ice retreat. Geophysical Research Letters, 37(1): L01602

Wu Bingyi, Wang Jia, Walsh J E. 2006. Dipole Anomaly in the winter Arctic atmosphere and its association with sea ice motion. Journal of Climate, 19(2): 210–225, doi: 10.1175/JCLI3619.1

Yao Yao, Luo Dehai, Dai Aiguo, et al. 2017. Increased quasi stationarity and persistence of Winter Ural blocking and Eurasian extreme cold events in response to Arctic warming: Part I. Insights from observational analyses. Journal of Climate, 30(10): 3549–3568, doi: 10.1175/JCLI-D-16-0261.1

Yao Yao, Luo Dehai, Zhong Linhao. 2018. Effects of northern hemisphere atmospheric blocking on Arctic sea ice decline in winter at weekly time scales. Atmosphere, 9(9): 331, doi: 10.3390/atmos9090331

Yoo C, Feldstein S B, Lee S. 2014. The prominence of a tropical convective signal in the wintertime Arctic temperature. Atmospheric Science Letters, 15(1): 7–12, doi: 10.1002/asl2.455

Zhang Xiangdong, He Juanxiong, Zhang Jing, et al. 2012. Enhanced poleward moisture transport and amplified northern high-latitude wetting trend. Nature Climate Change, 3(1): 47–51

Zhang Xiangdong, Ikeda M, Walsh J E. 2003. Arctic sea ice and freshwater changes driven by the atmospheric leading mode in a coupled sea ice-ocean model. Journal of Climate, 16(13): 2159–2177, doi: 10.1175/2758.1

Zhang Xiangdong, Sorteberg A, Zhang Jing, et al. 2008. Recent radical shifts of atmospheric circulations and rapid changes in Arctic climate system. Geophysical Research Letters, 35(22): L22701, doi: 10.1029/2008GL035607